Letter

Tunable electronic and magnetic phases in layered ruthenates: Strained $SrRuO_3$-$SrTiO_3$ heterostructures

Minjae Kim,[1,*] Chang-Jong Kang,[2,†] Jae-Ho Han,[3] Kyoo Kim,[4] and Bongjae Kim[5,‡]

[1]*Korea Institute for Advanced Study, Seoul 02455, South Korea*
[2]*Department of Physics, Chungnam National University, Daejeon 34134, South Korea*
[3]*Center for Theoretical Physics of Complex Systems, Institute for Basic Science (IBS), Daejeon 34126, South Korea*
[4]*Korea Atomic Energy Research Institute (KAERI), Daejeon 34057, South Korea*
[5]*Department of Physics, Kunsan National University, Gunsan 54150, South Korea*

(Received 11 August 2022; accepted 24 October 2022; published 3 November 2022)

Layered ruthenates are a unique class of systems which manifest a variety of electronic and magnetic features from competing energy scales. At the heart of such features lies multi-orbital physics, especially orbital-selective behavior. Here, we propose that the $SrRuO_3$-$SrTiO_3$ heterostructure is a highly tunable platform to obtain the various emergent properties. Employing the density functional theory plus dynamical mean-field theory, we thoroughly investigate the orbital-dependent physics of the system and identify the competing magnetic fluctuations. We show that the epitaxial strain drives the system towards multi-orbital or orbital selective Mott phases from the Hund metal regime. At the same time, the two different types of static magnetism, ferromagnetism and checkerboard antiferromagnetism, are stabilized from the competition with the spin-density wave instability.

DOI: 10.1103/PhysRevB.106.L201103

Introduction.–Various physical phenomena found in the layered ruthenates have attracted great interest from the condensed matter physics community. One of the representative materials is Sr_2RuO_4. It shows a strange metallic behavior, interpreted as a Hund metal phase in high temperatures ($\gtrsim$25 K) [1–5], and becomes an unconventional superconducting state in low temperatures ($\lesssim$1.5 K) [6]. In the metallic phase, it is a paramagnet with various magnetic fluctuations [7]. These magnetic fluctuations are thought to be involved as a pairing mechanism of the superconducting state [7–9], but the exact form of the order parameter is still under dispute almost thirty years after its finding [10]. Alternately, another representative material, Ca_2RuO_4, shows totally different physical properties despite being isovalent to Sr_2RuO_4. The ground state is a Mott insulator with a static antiferromagnetic order [11,12]. In between the two systems, $Sr_{2-x}Ca_xRuO_4$, one can find unusual structural, electric, and magnetic phases which includes heavy fermionic phases and crossovers of local and itinerant magnetism [11,13–15].

One essential source for such interesting behaviors is the multi-orbital nature of the ruthenates. The orbital-selective electronic correlations and Hund interactions within t_{2g} manifold are found to be responsible for the emergent properties such as Hund metal and diverse magnetic phases in the ruthenates [1,2,7,11,12,16–20]. For example, in $Ca_{1.8}Sr_{0.2}RuO_4$, the orbital-selective feature is well-identified both from the angle-resolved photoemission spectroscopy and various theoretical frameworks [15,21–23]. This multi-orbital nature makes ruthenates ideal systems for studying the balance and interplay of multiple competing physical parameters, such as bandwidth, inter- and intra-orbital correlation, crystal field splitting, and spin-orbit coupling [2]. In reality, however, there are not many materials other than the aforementioned ones, Sr_2RuO_4, Ca_2RuO_4, and inbetween ($Sr_{2-x}Ca_xRuO_4$), to be compared with theoretical models on the t_{2g} manifold.

The recent development of the oxide heteroepitaxy has offered a controllable route to tune the physical parameters of materials. Employing ample substrates, one can delicately grow the oxides under various strains with either compressive or tensile way, which enables the control of crystal field splitting, hopping anisotropy, and strength of the correlation [24,25]. Especially for strontium ruthenates, experimental demonstrations are readily made with single-layer ruthenates, which is achieved by sandwiching one layer of $SrRuO_3$ between $SrTiO_3$ blocks [26,27]. This has prompted the idea of possible tuning of the magnetism using external stimulus such as doping [28]. Previously, within the density functional theory (DFT) framework, some of the authors have demonstrated $(SrRuO_3)_1$-$(SrTiO_3)_1$ heterostructure (SRO-STO) as a possible system to study the superconductivity of Sr_2RuO_4 based on the similarity of quasi one-dimensional xz/yz and quasi two-dimensional xy Fermi surfaces to those from Sr_2RuO_4 [29]. It is interesting to investigate whether the conclusions are valid beyond the DFT framework known as an incomplete description of many-body correlation effects. Especially for ruthenates, the inclusion of the many-body effect is crucial in describing the key electronic features such as Hund-metal, band-renormalization, and metal-insulator

*garix.minjae.kim@gmail.com
†cjkang87@cnu.ac.kr
‡bongjae.kim@kunsan.ac.kr

transition [1,4,5,18,30–32], which, in turn, will change the relative strengths of the different magnetism. Considering the prospect of heteroengineering of ruthenates, there lies a plethora of physics that is yet to be discovered through the state-of-the-art computational approaches.

In this Letter, we investigate the electronic and magnetic structures of SRO-STO within the framework of DFT plus dynamical mean-field theory (DFT+DMFT) [33–36] for various epitaxial strain and temperature ranges. We demonstrate that the epitaxial strain controls the orbital-selective electronic correlation and moves the system toward two distinct Mott phase, multi-orbital, and orbital selective ones away from the Hund phase. An even more interesting point is that the strain can tune the strength of the different types of magnetic instabilities and lead to the stabilization of ferromagnetic (FM) or checkerboard-type antiferromagnetic (AFM) orders over spin-density wave (SDW) ones. Here, for completeness, we have employed two different but representative setups in the DMFT approach, and we map out the full strain-temperature phase diagram of SRO-STO system.

Method.–We compute the electronic structure of SRO-STO under epitaxial strains of -4%, 0%, and $+4\%$ within the DFT+DMFT framework. We have employed both Ru t_{2g} only and t_{2g}+e_g projected basis sets for the DFT+DMFT calculations to check the possible effect of $t_{2g} - e_g$ hybridization and confirmed that both give similar results for spectral functions $A(k, \omega)$ and density of state $A(\omega) = \sum_k A(k, \omega)$, see more details in Supplemental Material (SM) [37] (see also references [38–49] therein). The DMFT dynamical spin structure factors $S(q, \omega)$ are obtained in the paramagnetic (PM) phase of SRO-STO with Ru t_{2g}+e_g projector scheme [50], which covers a wide energy window of $[-10, 10]$ eV from the Fermi level (E_F). Based on the observation that the spectral functions from the t_{2g} and the t_{2g}+e_g projector schemes are consistent (see SM [37]), we present results with the t_{2g} projector scheme unless specified in the text.

Electronic correlation and orbital selectivity.–First, we present the electronic structure of the PM state of unstrained SRO-STO (0% strain) at $T = 35$ K. Figures 1(a) and (b) display related spectral function $A(k, \omega)$ and its integration over Brillouin zone $A(\omega)$, respectively. A coherent quasiparticle band is clearly realized near E_F, which has a quasi-two dimensional Ru xy-orbital character, exhibiting the van Hove singularity (VHS) [see Fig. 1(b)]. This VHS peak in the unstrained SRO-STO system is much higher than that of Sr_2RuO_4 [51]. Hence, enhanced Stoner weight at E_F, and consequently, the stronger tendency towards magnetism is expected for SRO-STO. In addition, the VHS peak in the SRO-STO system is located just below E_F, which is the *opposite* to the case of Sr_2RuO_4. Such features could lead to the different electronic and magnetic responses upon external perturbations in the SRO-STO system compared to previously investigated Sr_2RuO_4 [52,53]. The DMFT valence histogram of the unstrained SRO-STO system exhibits Hund's rule-induced high spin multiplets (see SM [37]), thereby presenting the Hund metal characteristics. Especially, we note two archetypical features: (i) coherence-incoherence crossover as a function of frequency ω in the

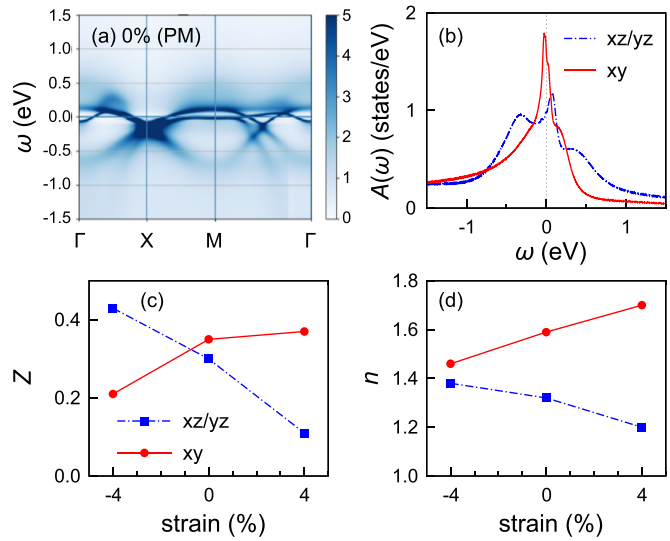

FIG. 1. (a) The spectral function $A(k, \omega)$ and (b) orbitally resolved density of state $A(\omega)$ of the unstrained SRO-STO (0% strain). Strain dependent (c) quasiparticle residues, Z, and (d) occupancies, n, for xz/yz and xy orbitals. The nonmagnetic constraint is forced to simulate the paramagnetism (PM) with the temperature of 35 K for all data.

self-energy $\Sigma(\omega)$ (see SM [37]), and (ii) significant electronic correlations in the absence of the Hubbard satellite. The significant electronic correlations are clearly identified in the quasiparticle residue, $Z = (1 - \partial\Sigma(i\omega)/\partial\omega|_{\omega\to 0^+})^{-1}$, and Ru xz/yz and xy have $Z = 0.30$ and 0.35, respectively [see Fig. 1(c)], which are comparable to the values of Sr_2RuO_4, 0.30 (xz/yz) and 0.20 (xy) [51]. We see the overall electronic features resemble those for Sr_2RuO_4 despite the small differences.

Remarkably, the SRO-STO exhibits diverse electronic phases within an accessible strain range. The epitaxial strain imposes a tetragonal distortion, and the energy difference between the Ru xz/yz and xy levels varies under the strain. Figure 1(c) displays the strain-dependent quasiparticle residue Z for Ru xz/yz and xy orbitals. We note the different responses of Z upon tensile strain: decreases for xz/yz orbitals and increases for xy orbital. This orbital differentiation is clearly reflected in the orbital occupancy as shown in Fig. 1(d). For the compressive strain, the xy level moves higher in energy and approaches the xz/yz levels (see SM [37]). As a result, the xy-orbital occupation is reduced, and the VHS moves even closer to E_F, indicating stronger FM instability. These features give rise to the reduction of the low-energy hybridization function for the xy orbital and, hence, increase the electronic correlations in the xy orbital as shown in Fig. 1(c). This can be compared to $Ca_{1.8}Sr_{0.2}RuO_4$ [23], where the xy orbital has an occupancy close to the half-filling and possess a stronger electronic correlation than xz/yz orbitals [23]. For $Ca_{1.8}Sr_{0.2}RuO_4$, the orbital selective Mott-phase is established with gapped xy orbital and metallic xz/yz orbitals [15,21–23]. Hence, we argue that the electronic structure of the compressed SRO-STO system corresponds to the *soft* case of $Ca_{1.8}Sr_{0.2}RuO_4$.

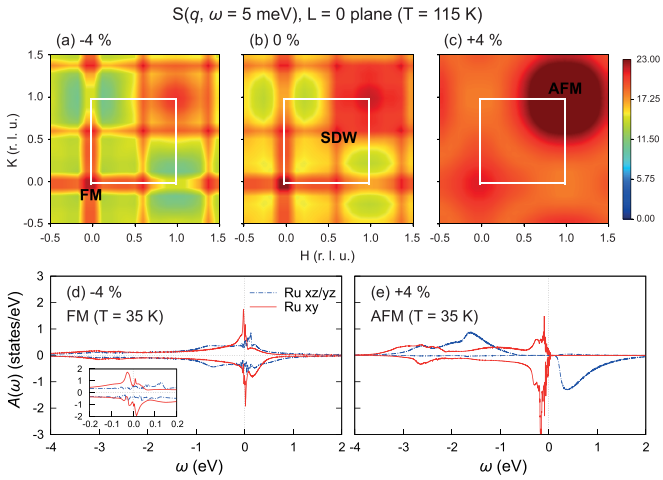

FIG. 2. Momentum (q) dependent dynamical structure factors $S(q, \omega)$ of SRO-STO for (a) -4%, (b) 0%, and (c) $+4\%$ strain cases. Here, for $S(q, \omega)$, the t_{2g}+e_g projector calculation is performed, and the data is for $\omega = 5$ meV at the temperature of 115 K. In the lower panels, we present the spin-resolved density of states for (d) FM -4% strain and (e) AFM $+4\%$ strain cases at 35 K. The inset in (d) is the blowup figure near the Fermi level.

In the case of tensile strains ($+4\%$), the Ru xy level moves down in energy, and the crystal field splitting between the xz/yz and xy levels becomes larger (see SM [37]). Accordingly, the occupation of the xz/yz orbitals decreases, while that of the xy orbital increases. Contrary to the compressive case, this time the Z for xz/yz orbitals is 0.11 with the orbital occupation close to the half-filling, 1.20 [see Figs. 1(c) and 1(d)]. This means the tensile strain drives the system towards the multi-orbital Mott regime [37,54]. The multi-orbital Mott insulating regime is found in Ca_2RuO_4, where the fully-filled xy and half-filled xz/yz orbitals are realized with a prominent Mott gap of $U + J$ (~ 2.7 eV) [18].

Magnetism.–Now we turn to the magnetic properties of the SRO-STO system. To identify the involved magnetic instabilities, we calculated the DMFT dynamical spin structure factors $S(q, \omega)$ with the local particle-hole vertex correction [50]. The results are presented in Figs. 2(a)–2(c). For the unstrained one, three leading competing magnetic instabilities are identified: FM at Γ $(H, K) = (0.0, 0.0)$, SDW at $(H, K) = (\sim 0.6, \sim 0.6)$, and checkerboard AFM at $(H, K) = (1.0, 1.0)$. Note that the last instability, AFM, is not captured in the DFT level [29], which asserts the importance of the dynamical correlations in describing the magnetism of the system. Each of the magnetic instabilities is from the different origins: FM from Stoner instability, SDW from Fermi surface nesting of quasi-1D yz/zx character, and AFM from superexchange mechanism [8]. These magnetic instabilities compete without specific dominance and the system remains paramagnetic without static order. Note that for Sr_2RuO_4, two main magnetic instabilities are featured, FM and SDW types, and for Ca_2RuO_4, only AFM is stabilized [7,12,17]. Hence, we can note that the magnetism involved in the SRO-STO system is even more complex, and also offers more possibilities for the novel phases including unconventional superconductivity.

For compressive strain (-4%), the FM instability becomes strongly dominant. As mentioned before, this is expected as the VHS peak, mostly from the xy orbital, moves closer to E_F upon the compressive strain (see SM [37]) and the Stoner instability increases accordingly. As shown in Fig. 2(a), the AFM instability is strongly suppressed, and the SDW instability has a similar amplitude. Compared to the unstrained one, the FM tendency in the compressive strain is substantially enhanced and much more predominant concerning the AFM and the SDW. Hence, the static FM order is set in for the compressive SRO-STO. We have confirmed that the actual DFT+DMFT calculations converge to the FM ground state under the compressive strain. The orbital-resolved $A(\omega)$ for the FM ground state is shown in Fig. 2(d) at $T = 35$ K. The exchange splitting $[\mathrm{Re}\Sigma_\downarrow(0)\text{-}\mathrm{Re}\Sigma_\uparrow(0)]$ in the Ru xy orbital (199 meV) is larger than that in the Ru xz/yz orbitals (79 meV) [see the inset of Fig. 2(d)]. This confirms that the Ru xy orbital drives the magnetic transition *via* the Stoner mechanism. The nonvanishing magnetic moment started to emerge around $T = 100$ K and the value progressively increases as T decreases, thereby suggesting the second-order magnetic transition [37]. Our obtained magnetic moment is ~ 0.35 μ_B, which is close to the experimental report from the ferromagnetic $(SrRuO_3)_1$-$(SrTiO_3)_5$ [27]. The saturated moment is much smaller than the ionic value of 2 μ_B, implying the highly itinerant character of the FM.

For the tensile strain of $+4\%$, the AFM instability strongly prevails and both the FM and the nesting-induced SDW ones are almost buried under the AFM instability as shown in Fig. 2(c). The DMFT density of states $A(\omega)$ at $\omega = 0$ (E_F) is reduced from -4% (compressive) to the 4% (tensile) strains (see SM [37]), which manifests the dwindling of the Stoner instability. This is expected considering the increased interatomic distances between Ru, which reduced the itinerancy of the system. Besides, we note the SDW Fermi surface nesting is significantly weaker under $+4\%$ strain (see SM [37]). Interestingly, in Ref. [28], a small carrier doping can turn the system into a FM metal, which can be an efficient way to again achieve the FM metallic phase. Such a stark variation of the magnetism upon the external perturbation is very unique, especially in the sense that the other competing magnetic instabilities, except for the AFM, are almost annulled. To confirm, we additionally performed the DMFT electronic structure calculations and found that the AFM phase is the ground state under the tensile strain as found from the $S(q, \omega)$ (see SM [37]). This strong emergence of the checkerboard AFM instability asserts that the mechanism of the magnetic order now is superexchange interactions between the *local* Ru spins. Figure 2(e) shows related orbital-resolved $A(\omega)$ at $T = 35$ K. The AFM ground state is an insulating phase with fully occupied Ru xy and half-filled Ru xz/yz orbitals. The local magnetic moment is about 1.87 μ_B/Ru and remained almost constant below the Néel temperature of ~ 100 K, suggesting the first-order type transition. This is totally different from the FM for compressive strain, where the local moment size develops upon decreasing the temperatures. We can compare the electronic structure and magnetism of the AFM insulating state of SRO-STO under

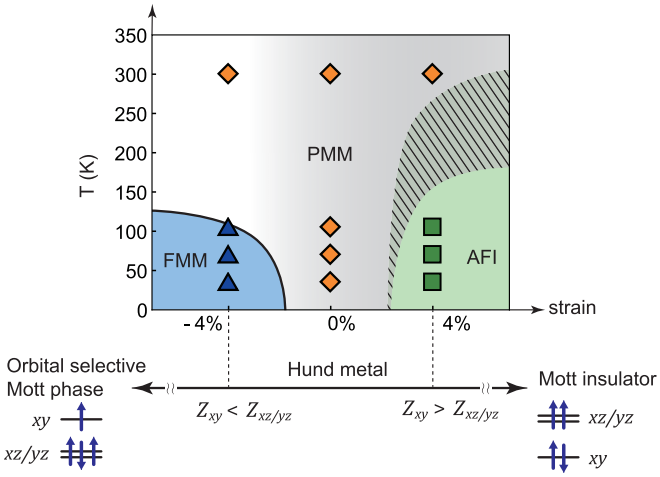

FIG. 3. Temperature-strain dependent phase diagram of SRO-STO. The DFT+DMFT results are denoted by blue triangle, orange rhombus, and green square for FM metallic phase (FMM), PM metallic phase (PMM), and AFM insulating (AFI) phase, respectively. The gradient from gray to white color shows the variation of Z_{xy} and $Z_{xz/yz}$ values, $Z_{xy} > Z_{xz/yz}$ (dark region) and $Z_{xy} < Z_{xz/yz}$ (light region). The phase boundaries are drawn schematically. The hatched region between AFI and PMM phases indicates asserted first order phase transition. Limiting cases are multi-orbital Mott insulating phase with half-filled (fully filled) xz/yz (xy) orbital ($Z_{xy} > Z_{xz/yz}$), and orbital selective Mott phase having the half-filled (3/2 filled) xy (xz/yz) orbital ($Z_{xy} < Z_{xz/yz}$).

the tensile strain to those of the multi-orbital Mott insulating phase of Ca_2RuO_4 at low temperatures, having a similar electronic configuration, half-filled xz/yz and fully filled xy orbitals.

Phase diagram.–By collecting all the data on the electronic and magnetic properties, we finally construct a comprehensive strain-temperature phase diagram of the SRO-STO system (see Fig. 3). It is illustrated that the strain-induced variation of the crystal field splitting is an essential physical parameter for emergent quantum phases. In the tensile (compressive) strain, the xz/yz (xy) orbital energy level is lifted up with respect to the xy (xz/yz) orbital, driving the system toward the multi-orbital Mott insulator (orbital selective Mott phase). This strain induced manipulation of physical regimes in SRO-STO is related to the emergence of various magnetism.

Our phase diagram in Fig. 3 introduces two accessible routes for the magnetic phase transition employing the epitaxial strain engineering starting from the paramagnetic Hund metal phase of the unstrained system. First, by applying the compressive strain, one reaches the FM metal phase from the competition with the SDW and the AFM phases. This is very interesting because, while there are a few reports on the static magnetism upon doping or external perturbation [14,55–57], due to the fragile nature of FM, most of them are AFM or SDW and no FM has been stabilized for layered ruthenates. Together with orbital-selective characteristic of the compressive case, this phase can offer unreported areas for further studies. Note that $SrRuO_3$ is also a FM metal, but the system is a three-dimensional one and has a much milder electronic correlation [16,58,59]. When the tensile strain is applied, the other magnetic instabilities are quickly muted and a checkerboard AFM phase with a strong insulating electronic structure can be obtained. This phase is similar to the one from Ca_2RuO_4. As the temperature is increased, the system goes through the first-order type transition into the PM metal phase. We expect that there exists a coexistence phase of PM metal and AFM insulator based on the first-order type transition and unattainable convergence, which is denoted as the shaded area in Fig. 3. This is very different to the compressive strain case, where the FM transition is expected to be a second-order one. The different mechanisms of magnetism can be a reason for the contrasting transition, (i) the *itinerant* Stoner mechanism induced FM emerges in the metallic phase and (ii) the *local* superexchange mechanism induced AFM emerges in the insulating phase. We note that the AFM insulating phase for the tensile strain emerges with the enhancement of the orbital polarization, having nearly integer filling of $n_{xz/yz} = 1.01$ and $n_{xy} = 2.00$, in comparison with the noninteger filling in the PM metallic phase of the tensile strain in Fig. 1(d). On the other hand, the FM metallic phase for the compressive strain emerges without changes of the orbital occupation in comparison with the noninteger filling for the PM metallic phase of the compressive strain in Fig. 1(d).

Conclusion.–We have investigated the strain-temperature dependent electronic and magnetic properties of the SRO-STO heterostructure system within the DFT+DMFT method. When unstrained, the system has a slightly enhanced magnetic tendency with a similar degree of electronic correlation over bulk layered counterparts. However, such a small difference enables a plethora of interesting phases when combined with the workable epitaxial strain. We presented the strain-temperature phase diagram of the SRO-STO system, which can access various electronic and magnetic phases observed from the diverse bulk layered system as well as the unreported magnetic and electronic phases such as FM metal with orbital-selectiveness. We expect our work can guide the future experimental and theoretical directions towards the engineering of the layered ruthenates, and other correlated systems with competing physical energy scales.

Acknowledgments. The authors would like to acknowledge the support from Advanced Study Group program from PCS-IBS. M.K. was supported by KIAS Individual Grants(CG083501). C.J.K. was supported by the NRF (Grant No. 2022R1C1C1008200) and KISTI Supercomputing Center (Project No. KSC-2021-CRE-0580). B.K. acknowledges support by NRF Grants No. 2021R1C1C1007017 and No. 2022M3H4A1A04074153, and KISTI supercomputing Center (Project No. KSC-2021-CRE-0605). J.H.H. acknowledges financial support from the Institute for Basic Science in the Republic of Korea through the project IBS-R024-D1. K.K. is supported by KAERI internal R&D Program (Grant No. 524460-22). Part of the calculation is supported by the CAC at KIAS.

M. Kim and C.-J. Kang contributed equally to this work.

[1] J. Mravlje, M. Aichhorn, T. Miyake, K. Haule, G. Kotliar, and A. Georges, Coherence-Incoherence Crossover and the Mass-Renormalization Puzzles in Sr_2 RuO_4, Phys. Rev. Lett. **106**, 096401 (2011).

[2] A. Georges, L. de' Medici, and J. Mravlje, Strong correlations from Hund's coupling, Annu. Rev. Condens. Matter Phys. **4**, 137 (2013).

[3] A. Tamai, M. Zingl, E. Rozbicki, E. Cappelli, S. Riccò, A. de la Torre, S. McKeown Walker, F. Y. Bruno, P. D. C. King, W. Meevasana, M. Shi, M. Radović, N. C. Plumb, A. S. Gibbs, A. P. Mackenzie, C. Berthod, H. U. R. Strand, M. Kim, A. Georges, and F. Baumberger, High-Resolution Photoemission on Sr_2 RuO_4 Reveals Correlation-Enhanced Effective Spin-Orbit Coupling and Dominantly Local Self-Energies, Phys. Rev. X **9**, 021048 (2019).

[4] M. Kim, J. Mravlje, M. Ferrero, O. Parcollet, and A. Georges, Spin-Orbit Coupling and Electronic Correlations in Sr_2 RuO_4, Phys. Rev. Lett. **120**, 126401 (2018).

[5] G. Zhang, E. Gorelov, E. Sarvestani, and E. Pavarini, Fermi Surface of Sr_2 RuO_4: Spin-Orbit and Anisotropic Coulomb Interaction Effects, Phys. Rev. Lett. **116**, 106402 (2016).

[6] Y. Maeno, H. Hashimoto, K. Yoshida, S. Nishizaki, T. Fujita, J. G. Bednorz, and F. Lichtenberg, Superconductivity in a layered perovskite without copper, Nature (London) **372**, 532 (1994).

[7] P. Steffens, Y. Sidis, J. Kulda, Z. Q. Mao, Y. Maeno, I. I. Mazin, and M. Braden, Spin Fluctuations in Sr_2 RuO_4 from Polarized Neutron Scattering: Implications for Superconductivity, Phys. Rev. Lett. **122**, 047004 (2019).

[8] I. I. Mazin and D. J. Singh, Competitions in Layered Ruthenates: Ferromagnetism versus Antiferromagnetism and Triplet versus Singlet Pairing, Phys. Rev. Lett. **82**, 4324 (1999).

[9] A. T. Rømer, A. Kreisel, M. A. Müller, P. J. Hirschfeld, I. M. Eremin, and B. M. Andersen, Theory of strain-induced magnetic order and splitting of T_c and T_{trsb} in Sr_2 RuO_4, Phys. Rev. B **102**, 054506 (2020).

[10] A. P. Mackenzie, T. Scaffidi, C. W. Hicks, and Y. Maeno, Even odder after twenty-three years: The superconducting order parameter puzzle of Sr_2 RuO_4, npj Quantum Mater. **2**, 40 (2017).

[11] S. Nakatsuji, S.-i. Ikeda, and Y. Maeno, Ca_2 RuO_4 : New mott insulators of layered ruthenate, J. Phys. Soc. Jpn. **66**, 1868 (1997).

[12] M. Braden, G. André, S. Nakatsuji, and Y. Maeno, Crystal and magnetic structure of Ca_2 RuO_4: Magnetoelastic coupling and the metal-insulator transition, Phys. Rev. B **58**, 847 (1998).

[13] O. Friedt, M. Braden, G. André, P. Adelmann, S. Nakatsuji, and Y. Maeno, Structural and magnetic aspects of the metal-insulator transition in Ca_{2-x} Sr_x RuO_4, Phys. Rev. B **63**, 174432 (2001).

[14] J. P. Carlo, T. Goko, I. M. Gat-Malureanu, P. L. Russo, A. T. Savici, A. A. Aczel, G. J. MacDougall, J. A. Rodriguez, T. J. Williams, G. M. Luke, C. R. Wiebe, Y. Yoshida, S. Nakatsuji, Y. Maeno, T. Taniguchi, and Y. J. Uemura, New magnetic phase diagram of $(Sr,Ca)_2$ RuO_4, Nat. Mater. **11**, 323 (2012).

[15] M. Kim, J. Kwon, C. H. Kim, Y. Kim, D. Chung, H. Ryu, J. Jung, B. S. Kim, D. Song, J. D. Denlinger *et al.*, Signature of kondo hybridisation with an orbital-selective mott phase in 4*d* Ca_{2-x} Sr_x RuO_4, npj Quantum Mater. **7**, 1 (2022).

[16] H. T. Dang, J. Mravlje, A. Georges, and A. J. Millis, Electronic correlations, magnetism, and Hund's rule coupling in the ruthenium perovskites $SrRuO_3$ and $CaRuO_3$, Phys. Rev. B **91**, 195149 (2015).

[17] H. U. R. Strand, M. Zingl, N. Wentzell, O. Parcollet, and A. Georges, Magnetic response of Sr_2 RuO_4: Quasi-local spin fluctuations due to Hund's coupling, Phys. Rev. B **100**, 125120 (2019).

[18] D. Sutter, C. Fatuzzo, S. Moser, M. Kim, R. Fittipaldi, A. Vecchione, V. Granata, Y. Sassa, F. Cossalter, G. Gatti *et al.*, Hallmarks of Hunds coupling in the Mott insulator Ca_2 RuO_4, Nat. Commun. **8**, 15176 (2017).

[19] E. Gorelov, M. Karolak, T. O. Wehling, F. Lechermann, A. I. Lichtenstein, and E. Pavarini, Nature of the Mott Transition in Ca_2 RuO_4, Phys. Rev. Lett. **104**, 226401 (2010).

[20] A. Liebsch and H. Ishida, Subband Filling and Mott Transition in Ca_{2-x} Sr_x RuO_4, Phys. Rev. Lett. **98**, 216403 (2007).

[21] A. Shimoyamada, K. Ishizaka, S. Tsuda, S. Nakatsuji, Y. Maeno, and S. Shin, Strong Mass Renormalization at a Local Momentum Space in Multiorbital $Ca_{1.8}$ $Sr_{0.2}$ RuO_4, Phys. Rev. Lett. **102**, 086401 (2009).

[22] M. Neupane, P. Richard, Z.-H. Pan, Y.-M. Xu, R. Jin, D. Mandrus, X. Dai, Z. Fang, Z. Wang, and H. Ding, Observation of a Novel Orbital Selective Mott Transition in $Ca_{1.8}$ $Sr_{0.2}$ RuO_4, Phys. Rev. Lett. **103**, 097001 (2009).

[23] D. Sutter, M. Kim, C. E. Matt, M. Horio, R. Fittipaldi, A. Vecchione, V. Granata, K. Hauser, Y. Sassa, G. Gatti *et al.*, Orbitally selective breakdown of Fermi liquid quasiparticles in $Ca_{1.8}$ $Sr_{0.2}$ RuO_4, Phys. Rev. B **99**, 121115(R) (2019).

[24] D. G. Schlom, L.-Q. Chen, C.-B. Eom, K. M. Rabe, S. K. Streiffer, and J.-M. Triscone, Strain tuning of ferroelectric thin films, Annu. Rev. Mater. Res. **37**, 589 (2007).

[25] B. Kim, P. Liu, J. M. Tomczak, and C. Franchini, Strain-induced tuning of the electronic coulomb interaction in 3*d* transition metal oxide perovskites, Phys. Rev. B **98**, 075130 (2018).

[26] P.-C. Wu, H. Song, Y. Yuan, B. Feng, Y. Ikuhara, R. Huang, P. Yu, C.-G. Duan, and Y.-H. Chu, Thickness dependence of transport behaviors in $SrRuO_3/SrTiO_3$ superlattices, Phys. Rev. Mater. **4**, 014401 (2020).

[27] H. Boschker, T. Harada, T. Asaba, R. Ashoori, A. V. Boris, H. Hilgenkamp, C. R. Hughes, M. E. Holtz, L. Li, D. A. Muller *et al.*, Ferromagnetism and Conductivity in Atomically Thin $SrRuO_3$, Phys. Rev. X **9**, 011027 (2019).

[28] L. Si, Z. Zhong, J. M. Tomczak, and K. Held, Route to room-temperature ferromagnetic ultrathin $SrRuO_3$ films, Phys. Rev. B **92**, 041108(R) (2015).

[29] B. Kim, S. Khmelevskyi, C. Franchini, I. I. Mazin, and K. Kim, $SrRuO_3$-$SrTiO_3$ heterostructure as a possible platform for studying unconventional superconductivity in Sr_2 RuO_4, Phys. Rev. B **101**, 220502(R) (2020).

[30] S. Riccò, M. Kim, A. Tamai, S. Mckeown Walker, F. Y. Bruno, I. Cucchi, E. Cappelli, C. Besnard, T. K. Kim, P. Dudin *et al.*, In situ strain tuning of the metal-insulator-transition of Ca_2 RuO_4 in angle-resolved photoemission experiments, Nat. Commun. **9**, 1 (2018).

[31] Q. Han and A. Millis, Lattice Energetics and Correlation-Driven Metal-Insulator Transitions: The Case of Ca_2 RuO_4, Phys. Rev. Lett. **121**, 067601 (2018).

[32] X. Deng, K. M. Stadler, K. Haule, A. Weichselbaum, J. von Delft, and G. Kotliar, Signatures of mottness and hundness in archetypal correlated metals, Nat. Commun. **10**, 1 (2019).

[33] A. Georges and G. Kotliar, Hubbard model in infinite dimensions, Phys. Rev. B **45**, 6479 (1992).

[34] W. Metzner and D. Vollhardt, Correlated Lattice Fermions in $d = \infty$ Dimensions, Phys. Rev. Lett. **62**, 324 (1989).

[35] G. Kotliar, S. Y. Savrasov, K. Haule, V. S. Oudovenko, O. Parcollet, and C. A. Marianetti, Electronic structure calculations with dynamical mean-field theory, Rev. Mod. Phys. **78**, 865 (2006).

[36] A. Georges, G. Kotliar, W. Krauth, and M. J. Rozenberg, Dynamical mean-field theory of strongly correlated fermion systems and the limit of infinite dimensions, Rev. Mod. Phys. **68**, 13 (1996).

[37] See Supplemental Material at http://link.aps.org/supplemental/10.1103/PhysRevB.106.L201103 for calculation details, comparison of two DMFT methods, discussion on Hund metallicity, Fermi surfaces, frequency dependent dynamical structure factors, strain effects on the Ru-O distances and the crystal field, temperature evolution of the magnetism.

[38] O. Parcollet, M. Ferrero, T. Ayral, H. Hafermann, I. Krivenko, L. Messio, and P. Seth, Triqs: A toolbox for research on interacting quantum systems, Comput. Phys. Commun. **196**, 398 (2015).

[39] M. Aichhorn, L. Pourovskii, P. Seth, V. Vildosola, M. Zingl, O. E. Peil, X. Deng, J. Mravlje, G. J. Kraberger, C. Martins *et al.*, TRIQS/DFTTools: A TRIQS application for *ab initio* calculations of correlated materials, Comput. Phys. Commun. **204**, 200 (2016).

[40] P. Seth, I. Krivenko, M. Ferrero, and O. Parcollet, Triqs/cthyb: A continuous-time quantum Monte Carlo hybridisation expansion solver for quantum impurity problems, Comput. Phys. Commun. **200**, 274 (2016).

[41] P. Blaha, K. Schwarz, F. Tran, R. Laskowski, G. K. Madsen, and L. D. Marks, WIEN2k: An APW+ lo program for calculating the properties of solids, J. Chem. Phys. **152**, 074101 (2020).

[42] K. Haule and G. Kotliar, Coherence–incoherence crossover in the normal state of iron oxypnictides and importance of Hund's rule coupling, New J. Phys. **11**, 025021 (2009).

[43] K. Haule, Quantum Monte Carlo impurity solver for cluster dynamical mean-field theory and electronic structure calculations with adjustable cluster base, Phys. Rev. B **75**, 155113 (2007).

[44] K. Haule, C.-H. Yee, and K. Kim, Dynamical mean-field theory within the full-potential methods: Electronic structure of $CeIrIn_5$, $CeCoIn_5$, and $CeRhIn_5$, Phys. Rev. B **81**, 195107 (2010).

[45] D. Stricker, J. Mravlje, C. Berthod, R. Fittipaldi, A. Vecchione, A. Georges, and D. van der Marel, Optical Response of Sr_2 RuO_4 Reveals Universal Fermi-Liquid Scaling and Quasiparticles Beyond Landau Theory, Phys. Rev. Lett. **113**, 087404 (2014).

[46] X. Deng, K. Haule, and G. Kotliar, Transport Properties of Metallic Ruthenates: A DFT+DMFT Investigation, Phys. Rev. Lett. **116**, 256401 (2016).

[47] J. P. Perdew, K. Burke, and M. Ernzerhof, Generalized Gradient Approximation Made Simple, Phys. Rev. Lett. **77**, 3865 (1996).

[48] E. Gull, A. J. Millis, A. I. Lichtenstein, A. N. Rubtsov, M. Troyer, and P. Werner, Continuous-time Monte Carlo methods for quantum impurity models, Rev. Mod. Phys. **83**, 349 (2011).

[49] P. Werner, A. Comanac, L. de' Medici, M. Troyer, and A. J. Millis, Continuous-Time Solver for Quantum Impurity Models, Phys. Rev. Lett. **97**, 076405 (2006).

[50] H. Park, K. Haule, and G. Kotliar, Magnetic Excitation Spectra in $BaFe_2$ As_2 : A Two-Particle Approach within a Combination of the Density Functional Theory and the Dynamical Mean-Field Theory Method, Phys. Rev. Lett. **107**, 137007 (2011).

[51] F. B. Kugler, M. Zingl, H. U. R. Strand, S.-S. B. Lee, J. von Delft, and A. Georges, Strongly Correlated Materials from a Numerical Renormalization Group Perspective: How the Fermi-Liquid State of Sr_2 RuO_4 Emerges, Phys. Rev. Lett. **124**, 016401 (2020).

[52] Y.-T. Hsu, W. Cho, A. F. Rebola, B. Burganov, C. Adamo, K. M. Shen, D. G. Schlom, C. J. Fennie, and E.-A. Kim, Manipulating superconductivity in ruthenates through Fermi surface engineering, Phys. Rev. B **94**, 045118 (2016).

[53] B. Kim, M. Kim, C.-J. Kang, J.-H. Han, and K. Kim, Competing spin-fluctuations in Sr_2 RuO_4 and their tuning through epitaxial strain, arXiv:2205.11711.

[54] Indeed, $A(\omega)$ for the xz/yz orbitals shows a hump at around ω=-1.38 eV, a typical signal for Mott phase, at the binding energy of $(U + J)/2$ (∼1.35 eV). Note that this hump feature only for the tensile strains case [37].

[55] V. Grinenko, S. Ghosh, R. Sarkar, J.-C. Orain, A. Nikitin, M. Elender, D. Das, Z. Guguchia, F. Brückner, M. E. Barber *et al.*, Split superconducting and time-reversal symmetry-breaking transitions in Sr_2 RuO_4 under stress, Nat. Phys. **17**, 748 (2021).

[56] M. Braden, O. Friedt, Y. Sidis, P. Bourges, M. Minakata, and Y. Maeno, Incommensurate Magnetic Ordering in Sr_2 Ru_{1-x} Ti_x O_4, Phys. Rev. Lett. **88**, 197002 (2002).

[57] B. Kim, S. Khmelevskyi, C. Franchini, and I. I. Mazin, Suppressed fluctuation as the origin of the static order in strained Sr_2 RuO_4, arXiv:2206.13826.

[58] M. Kim and B. I. Min, Nature of itinerant ferromagnetism of $SrRuO_3$: A DFT+DMFT study, Phys. Rev. B **91**, 205116 (2015).

[59] S. Hahn, B. Sohn, M. Kim, J. R. Kim, S. Huh, Y. Kim, W. Kyung, M. Kim, D. Kim, Y. Kim, T. W. Noh, J. H. Shim, and C. Kim, Observation of Spin-Dependent Dual Ferromagnetism in Perovskite Ruthenates, Phys. Rev. Lett. **127**, 256401 (2021).